Available online at www.sciencedirect.com
SCIENCE DIRECT®
Journal of Power Sources 119–121 (2003) 637–643
JOURNAL OF POWER SOURCES
www.elsevier.com/locate/jpowsour

Thermodynamic and kinetic approaches to lithium intercalation into $Li[Ti_{5/3}Li_{1/3}]O_4$ film electrode

Kyu-Nam Jung, Su-Il Pyun*, Sung-Woo Kim

Department of Materials Science and Engineering, Korea Advanced Institute of Science and Technology, 373-1 Guseong-Dong, Yuseong-Gu, Daejeon 305-701, South Korea

Abstract

Lithium intercalation into $Li[Ti_{5/3}Li_{1/3}]O_4$ film electrode in the two-phase coexistence was investigated from the thermodynamic and kinetic viewpoints. The electrode potential versus lithium content curve of the film electrode was theoretically calculated in consideration of the interactions between lithium ions based upon a lattice gas model with the Monte Carlo simulation. According to the model, it was proposed that a wide potential plateau indicating the coexistence of a Li-poor phase α and a Li-rich phase β is due to the repulsive interactions between lithium ions. From the analysis of the ac-impedance spectra in the coexistence of two phases α and β, it was confirmed that the fraction of α phase at the electrode surface and that fraction of β phase continuously decreases and increases, respectively, with increasing lithium content. The analysis of the current transient led to the conclusion that transport of lithium ions subjected to the repulsive interactions within the electrode is governed by the cell-impedance-controlled constraint at the electrode surface during the phase transformation between α and β phases.

Keywords: Cell-impedance-controlled lithium transport; Current transient; $Li[Ti_{5/3}Li_{1/3}]O_4$ film electrode; Monte Carlo simulation; Two-phase coexistence

1. Introduction

For several decades, most researches on lithium transport through the lithium intercalation compounds have been focussed on diffusion of lithium ions within the compounds, assuming that diffusion of lithium ions is the rate-controlling process of the lithium intercalation [1–4]. However, in our recent works [5–8] on the potentiostatic current transient measured experimentally and calculated theoretically by a finite-difference method [9], it has been proposed that lithium transport through the transition metal oxides is not controlled by diffusion of lithium ions but by the cell-impedance, i.e. the current is determined by the quotient of the potential difference between the electrode potential and the applied potential divided by the cell-impedance.

In particular, it has been reported that the appearance of the current plateau in the current transient is attributable to the phase transformation between the Li-poor phase α and the Li-rich phase β during the cell-impedance-controlled lithium transport in the two-phase coexistence region. However, the finite-difference method gives little information how a new phase α forms and grows in β matrix in the two-phase coexistence region during the lithium deintercalation and vice versa.

The cubic-spinel $Li[Ti_{5/3}Li_{1/3}]O_4$ has been known to exhibit two-phase coexistence in a wide range of lithium content because of the strong attractive interactions between lithium ions [10,11]. In the recent Monte Carlo studies [12,13], it has been found that those interactions between lithium ions strongly affect the thermodynamic and kinetic properties of $LiMn_2O_4$. It is thus necessary to take the interactions between lithium ions into account for a more understanding of the formation and growth of α and β phases during the cell-impedance-controlled lithium deintercalation and intercalation, respectively, by using the Monte Carlo method based upon the lattice gas model.

In this work, therefore, the lithium intercalation into and deintercalation from the $Li[Ti_{5/3}Li_{1/3}]O_4$ film electrode in the two-phase coexistence region were investigated from the thermodynamic and kinetic view points with the aid of the Monte Carlo method based upon the lattice gas model. For this purpose, the electrode potential versus lithium content curve and the ac-impedance spectra were analysed to discuss the phase transformation between α and β phases due to the repulsive interactions between lithium ions. In addition, the potentionstatic current transients were analysed to conclude that lithium transport accompanied by the phase transforma-

* Corresponding author. Tel.: +82-42-869-3319; fax: +82-42-869-3310.
E-mail address: sipyun@mail.kaist.ac.kr (S.-I. Pyun).

0378-7753/03/$ – see front matter © 2003 Elsevier Science B.V. All rights reserved.
doi:10.1016/S0378-7753(03)00192-7

tion of α to β and vice versa, is controlled by the cell-impedance.

2. Experimental

In order to prepare Li–Ti solution by sol–gel method, lithium acetylacetonate (Li[$CH_3COCH{=}(CO{-})CH_3$]) and titanium oxide acetylacetonate (OTi[$CH_3COCH{=}(CO{-})CH_3$]) were dissolved in 1-butanol and acetic acid, having a molar Li/Ti ratio of 4/5. This solution was mixed by stirring for 24 h, and then was degassed by ultrasonic cleaner for 5 min at room temperature in a glove box (MECAPLEX GB94, Switzerland) filled with purified Ar gas. After this, the sol was filtered with polytetrafluoroethylene (PTFE) membrane whose average pore size is 0.2 μm.

The resulting sol was spin-coated on 200 nm thick Pt current collector on one-side polished Al_2O_3 substrate (Japan Fine Ceramic) at 5000 rpm for 30 s, and then was dried at 350 °C over 12 min to evaporate solvents and organic materials. The above spin-coating and drying processes were successively repeated to control the film thickness. Finally, the crystalline $Li[Ti_{5/3}Li_{1/3}]O_4$ film electrode was obtained by annealing the as-deposited film at 750 °C for 1 h in air. From the X-ray diffraction (XRD) analysis, the crystal structure of the annealed $Li[Ti_{5/3}Li_{1/3}]O_4$ film was found to be the cubic-spinel with space group $Fd\bar{3}m$. The annealed film was characterised to be deposited to the thickness of ca. 130 nm by scanning electron microscopy.

A three-electrode electrochemical cell was employed for the electrochemical experiments. Both the reference and counter electrodes were constructed from the lithium foil (Foote Mineral, USA, purity 99.9%) and a 1 M solution of lithium perchlorate ($LiClO_4$) in propylene carbonate (PC) was used as the electrolyte. The area of the film electrode exposed to the electrolyte amounted to 1 cm^2.

The galvanostatic intermittent titration technique (GITT) was employed by using Solartron 1287 electrochemical interface (ECI). Applying a constant current of 20 μA cm^{-2} to the cell during 50 s upon charging–discharging, the resulting cell potential transients were recorded. The deviation from the ideal stoichiometry of $Li[Ti_{5/3}Li_{1/3}]O_4$, δ, was calculated from the mass of the oxide and the electrical charge that was transferred upon charging–discharging. In order to obtain uniform distribution of lithium ions over the electrode after interruption of the constant current, it is required about 1 h to reach equilibrium. After that the open circuit potential was simply recorded as an electrode potential.

Electrochemical impedance measurement was carried out by using Solartron 1255 frequency response analyser combined with Solartron 1287 ECI. The electrode was first maintained at a potential of 1.450–1.650 V_{Li/Li^+} for 5×10^3 s to attain an equilibrium potential, and then the ac-impedance spectra were measured on the film electrode by applying an ac-amplitude of 5 mV_{rms} over the frequency range from 100 mHz to 100 kHz.

The potentiostatic current transients were measured on the film electrode in a 1 M $LiClO_4$–PC solution by jumping the initial potential 1.450 V_{Li/Li^+} to the lithium extraction potential in the range of 1.525–1.650 V_{Li/Li^+} for 1×10^3 s. Prior to lithium extraction, the film electrode was maintained at the initial potential for a sufficiently long time, 5×10^3 s, to obtain a low steady-state current. All the electrochemical experiments were performed at 25 °C in the glove box filled with purified Ar gas.

3. Results and discussion

It is well known that a typical electrode potential curve measured on the $Li[Ti_{5/3}Li_{1/3}]O_4$ electrode shows a wide potential plateau near 1.560 V_{Li/Li^+} during both lithium intercalation and deintercalation [4,10,11]. According to the simple Frumkin isotherm [14,15], it is generally accepted that the occurrence of the potential plateau in the electrode potential curve indicates the coexistence of a Li-poor phase α and a Li-rich phase β, due to the strong attractive interactions between the intercalated lithium ions. Recently, from the Monte Carlo studies [12,13] on the $LiMn_2O_4$ electrode, it has been reported that the coexistence of the disordered and ordered phases is caused by the repulsive interactions between lithium ions. In this work, therefore, to elucidate the effect of interactions between lithium ions on the intercalation into and deintercalation from the $Li[Ti_{5/3}Li_{1/3}]O_4$ film electrode, we used the Monte Carlo method best suited for the lattice gas with the short-range interactions.

For the Monte Carlo simulation, we employed the lattice gas model for the crystal structure of the cubic-spinel $Li[Ti_{5/3}Li_{1/3}]O_4$ well established in the previous XRD analyses [10,11]: lithium ions intercalated into $Li_{1+\delta}[Ti_{5/3}Li_{1/3}]O_4$ occupy both 8(a) and 16(c) sites. In the cubic-spinel $Li[Ti_{5/3}Li_{1/3}]O_4$ ($\delta = 0$) only the 8(a) sites are occupied by lithium ions. By contrast, in the rock-salt $Li_2[Ti_{5/3}Li_{1/3}]O_4$ ($\delta = 1$) only the 16(c) sites are occupied by lithium ions. In this work, we considered the first- and the second-nearest pairwise interactions between lithium ions: each 8(a) site is adjacent to four first-nearest 16(c) sites and four second-nearest 8(a) sites, and each 16(c) site is surrounded by two first-nearest 8(a) sites and six second-nearest 16(c) sites.

According to the model, the Hamiltonian H of the lattice is defined as [12,13,16]

$$H = J_1 \sum_{ij} c_i c_j + J_2 \sum_{ik} c_i c_k + J_3 \sum_{jl} c_j c_l - (\varepsilon_{i,j} + \mu) \sum_{i,j} c_{i,j}, \quad (1)$$

where J_1 is the effective pairwise interaction parameter between the first-nearest neighbouring lithium ions in the 8(a) and 16(c) sites, J_2 the interaction parameter between the second-nearest neighbouring lithium ions in the same 8(a) sites, J_3 the interaction parameter between the second-nearest neighbouring lithium ions in the same 16(c) sites,

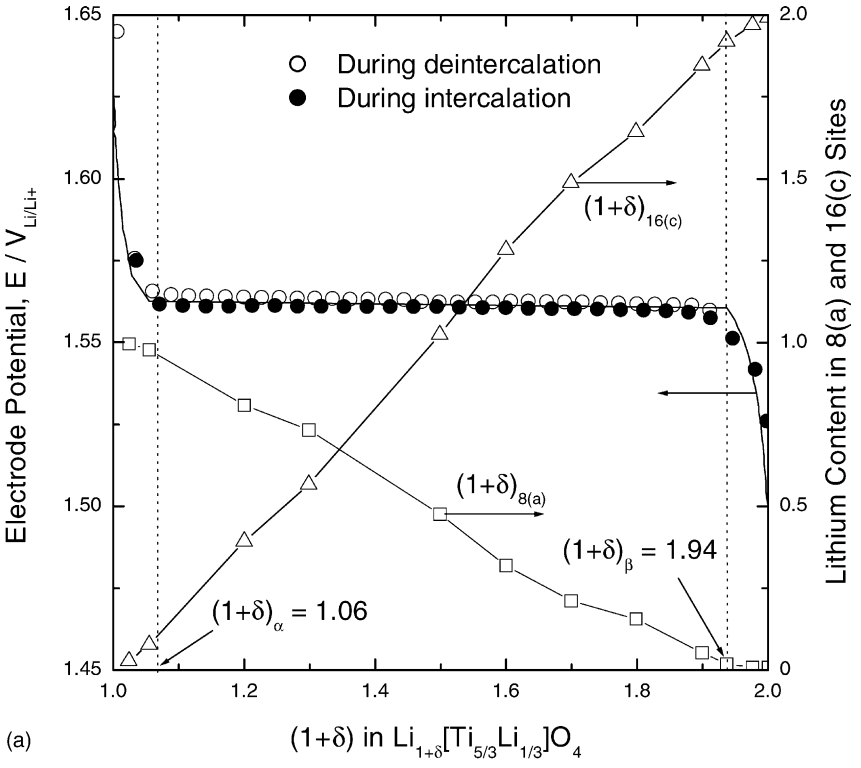

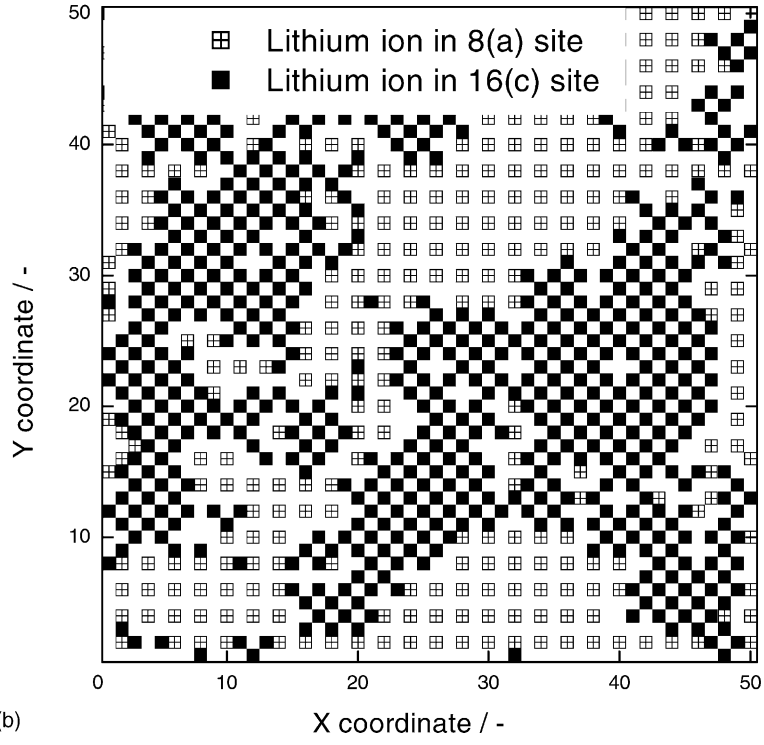

Fig. 1. (a) Electrode potential E vs. lithium content $(1+\delta)$ curve (solid line) and the plots of $(1+\delta)_{8(a)}$ (□) and $(1+\delta)_{16(c)}$ (△) with respect to $(1+\delta)$ theoretically calculated by the Monte Carlo method. (b) Local cross-sectional snapshot of the configuration of lithium ions at $(1+\delta)=1.50$. The electrode potential curves experimentally measured on the $Li_{1+\delta}[Ti_{5/3}Li_{1/3}]O_4$ film electrode during the lithium intercalation (●) and deintercalation (○) are also plotted.

ε_i and ε_j the effective binding energies of lithium ions in the 8(a) site i and the 16(c) site j, respectively, with titanium oxide matrix, μ the chemical potential of lithium ion, and c_i, c_j, c_k and c_l represent the local occupation numbers of the site i, j, k and l, respectively: if the site is occupied by lithium ions, c_i, c_j, c_k or $c_l = 1$, otherwise c_i, c_j, c_k or $c_l = 0$.

As a matter of fact, J_1, J_2 and J_3 cannot simply represent the direct interactions between lithium ions. In addition, the charge valences of the oxygen ions and the transition metal ions change during the lithium intercalation [17], indicating that ε_i and ε_j may change with lithium content. For the sake of simplicity, however, we performed the simulation under the assumption that those interaction parameters are independent of lithium content during lithium intercalation and deintercalation, because those interaction parameters lead us to successfully approximate the thermodynamic properties in this work. In the previous works, the effective values of those parameters were determined by fitting the electrode potential curve theoretically calculated to that curve experimentally measured [12,13,18] or by fitting the first-principle energy using local density approximation [19].

Under the circumstances, we approximately estimated the effective interaction parameters used in this work as follows: the effective values of J_2 and ε_i which are related to the interactions of lithium ions in the 8(a) sites, were determined to be 0.105 and 1.777 eV by fitting the electrode potential curve near $(1 + \delta) = 1$ where lithium ions are mainly located at the 8(a) sites; then the effective values of J_3 and ε_j which are concerned with the interactions of lithium ions in the 16(c) sites, amounted to 0.005 and 1.677 eV near $(1 + \delta) = 2$ where most lithium ions reside at the 16(c) sites; finally, the effective value of J_1 approximated to 0.110 eV in the potential plateau region.

It should be noted that the positive values of J_1, J_2 and J_3 used in this work mean the repulsive interactions between lithium ions. This is in contrast to the previous results reported by Ohzuku et al. [15]. They took the negative value of the effective interaction parameter indicating the attractive interactions according to the simple Frumkin isotherm under the assumption that lithium ions occupy only one kind of the site, which is not suited in this case.

Fig. 1(a) gives the electrode potential E versus lithium content $(1 + \delta)$ curves experimentally measured by GITT with open and closed circles, and E versus $(1 + \delta)$ curve theoretically calculated by the Monte Carlo method with solid line. For the calculation, we took $J_1 = 0.110$, $J_2 = 0.105$, $J_3 = 0.005$, $\varepsilon_i = 1.777$ and $\varepsilon_j = 1.677$ eV at $T = 298$ K, noting that $E = -\mu/e$ where e is the electronic unit charge. The electrode potential curve theoretically calculated showed the wide potential plateau in the range of $(1 + \delta) = 1.06$–1.94, which well coincided in value and shape with the electrode potential curves experimentally measured. Fig. 1(a) showed that lithium content in the 8(a) sites $(1 + \delta)_{8(a)}$ theoretically calculated decreases with increasing $(1 + \delta)$ in the potential plateau region, but that lithium content in the 16(c) sites $(1 + \delta)_{16(c)}$ increases. In order to explain the variations of $(1 + \delta)_{8(a)}$ and $(1 + \delta)_{16(c)}$ with $(1 + \delta)$ in terms of the phase transformation between α and β phases, the local cross-sectional snapshot of the configuration of lithium ions was simulated by the Monte Carlo method [13].

Fig. 1(b) envisages the local cross-sectional snapshot of the configuration of lithium ions theoretically obtained at $(1 + \delta) = 1.50$. It was easily seen that β phase which is in equilibrium with α phase, is sporadically embedded in α matrix. Here, α phase means the Li-poor region where lithium ions mainly reside in the 8(a) sites, and β phase represents the Li-rich region where most lithium ions occupy the 16(c) sites, to avoid the repulsive interactions between lithium ions that increase the ensemble energy of the lattice. From the results, it was confirmed that the wide potential plateau in the electrode potential curve means the two-phase coexistence of α and β phases due to the repulsive interactions between lithium ions. In addition, the variations of $(1 + \delta)_{8(a)}$ and $(1 + \delta)_{16(c)}$ with $(1 + \delta)$ may be closely related to those variations of the amount of α and β phases, respectively, in the two-phase coexistence.

The amounts of α and β phases in the two-phase coexistence region were experimentally determined by the analysis of the ac-impedance spectra measured on the $Li[Ti_{5/3}Li_{1/3}]O_4$ film electrode. Fig. 2(a) presents typical ac-impedance spectra in Nyquist plot composed of two separated arcs in the high and intermediate frequency ranges, a straight line inclined at constant angle to the real axis, and a capacitive line in the low-frequency range. In order to analyse the ac-impedance spectra, the equivalent circuit generally used for the intercalation electrode [20] was modified in this work. Fig. 2(b) illustrates the modified equivalent circuit, where R_u is the uncompensated Ohmic resistance of the electrolyte, R_1 and C_1 the high-frequency resistance and capacitance, respectively, $R_{2,i}$ and $C_{2,i}$ the intermediate frequency resistance associated with the lithium insertion (or absorption) and the interfacial capacitance, respectively, of the electrode composed of the phase i ($i = \alpha$ and β), θ_i the fraction of the amount of the phase i ($\theta_i \leq 1$; $\theta_\alpha + \theta_\beta = 1$), and $Z_{w,i}$ represents the finite length Warburg impedance of diffusion of lithium ions through the phase i.

Keeping in mind that β phase, which is in equilibrium with α phase, is sporadically embedded in α matrix during lithium intercalation, so it is readily expected that the intermediate frequency resistance is strongly affected by the fractions of the amounts of α and β phases at the electrode surface, θ_α and θ_β. According to the equivalent circuit, θ_α and θ_β were determined by complex nonlinear least squares (CNLS) fitting method [21] from the intermediate frequency resistances of α phase $R_{2,\alpha}$ and of β phase $R_{2,\beta}$ which were measured at $(1 + \delta)_\alpha$ and at $(1 + \delta)_\beta$, respectively. The θ_α and θ_β experimentally determined at various $(1 + \delta)$ are listed in Table 1. In the two-phase coexistence region θ_α monotonically decreased and θ_β increased with increasing $(1 + \delta)$ during lithium intercalation, while θ_α monotonically increased and θ_β decreased

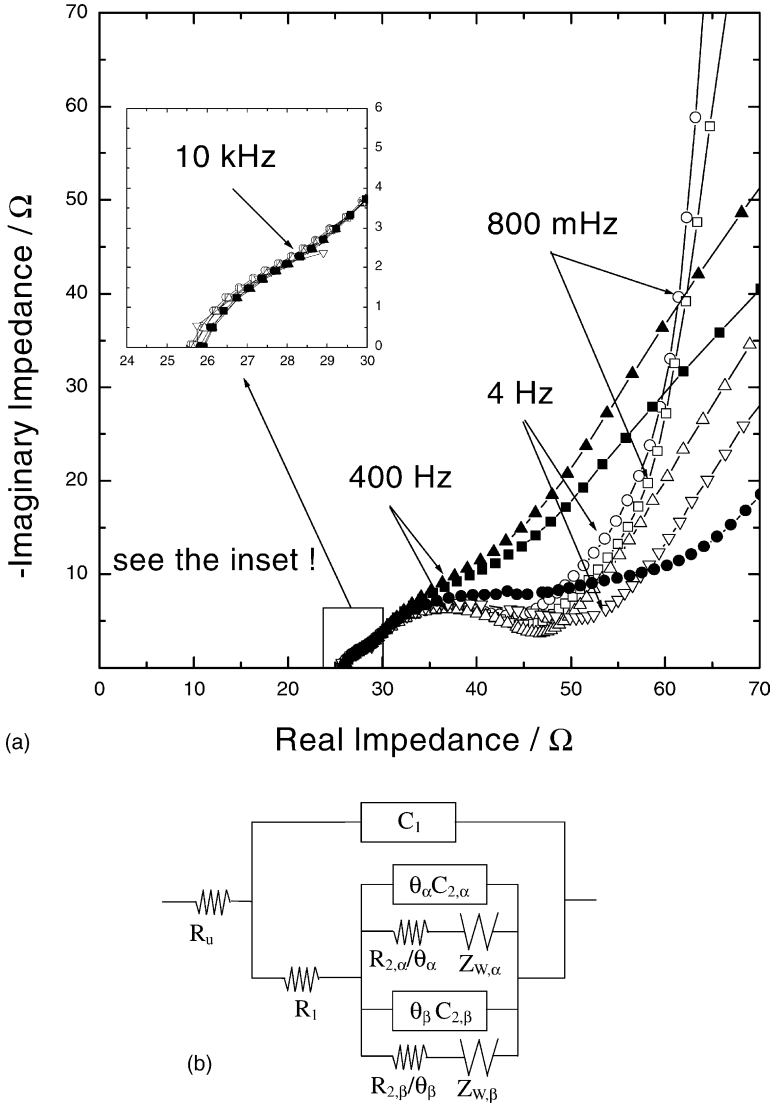

Fig. 2. (a) Nyquist plots of the ac-impedance spectra measured on the $Li_{1+\delta}[Ti_{5/3}Li_{1/3}]O_4$ film electrode in a 1 M $LiClO_4$–PC solution at various electrode potentials: (○) 1.650 V_{Li/Li^+}; (□) 1.600 V_{Li/Li^+}; (△) 1.560 V_{Li/Li^+} ($(1+\delta) = 1.17$); (▽) 1.560 V_{Li/Li^+} ($(1+\delta) = 1.46$); (●) 1.560 V_{Li/Li^+} ($(1+\delta) = 1.76$); (■) 1.500 V_{Li/Li^+}; (▲) 1.450 V_{Li/Li^+}. (b) The equivalent circuit used for the CNLS fitting method.

with decreasing $(1+\delta)$ during lithium deintercalation. It should be stressed that the result of the ac-impedance analysis in this work well coincided with the previous result of the XRD analysis [11].

Table 1
The fractions of the amounts of α and β phases at the electrode surface θ_α and θ_β, respectively, determined by the ac-impedance analysis during the lithium intercalation and deintercalation

Intercalation			Deintercalation		
$1+\delta$	θ_α	θ_β	$1+\delta$	θ_α	θ_β
1.17	0.84	0.16	1.84	0.20	0.80
1.31	0.68	0.32	1.70	0.30	0.70
1.46	0.60	0.40	1.56	0.35	0.65
1.62	0.47	0.53	1.43	0.45	0.55
1.76	0.35	0.65	1.29	0.53	0.47
1.90	0.23	0.77	1.16	0.73	0.27

Fig. 3 illustrates on a logarithmic scale the anodic current transients experimentally measured on the $Li[Ti_{5/3}Li_{1/3}]O_4$ film electrode in a 1 M $LiClO_4$–PC solution by jumping the initial potential 1.450 V_{Li/Li^+} to various lithium extraction potentials. All the current transients barely show Cottrell behaviour, i.e. they do not obey the linear relationship between logarithmic current and logarithmic time with a slope of −0.5 in the early stage. The current transients measured at the lithium extraction potentials 1.525 and 1.550 V_{Li/Li^+} below the plateau potential 1.560 V_{Li/Li^+}, showed a monotonic increase of its slope from the almost flat value to the infinite one in absolute value without any inflection point. However, the current transients on a logarithmic scale obtained at the potential jumps to 1.575, 1.600, 1.625 and 1.650 V_{Li/Li^+} through the plateau potential, ran with the slope flatter than −0.5 in the early stage, then exhibited a wide current plateau followed by an abrupt decay

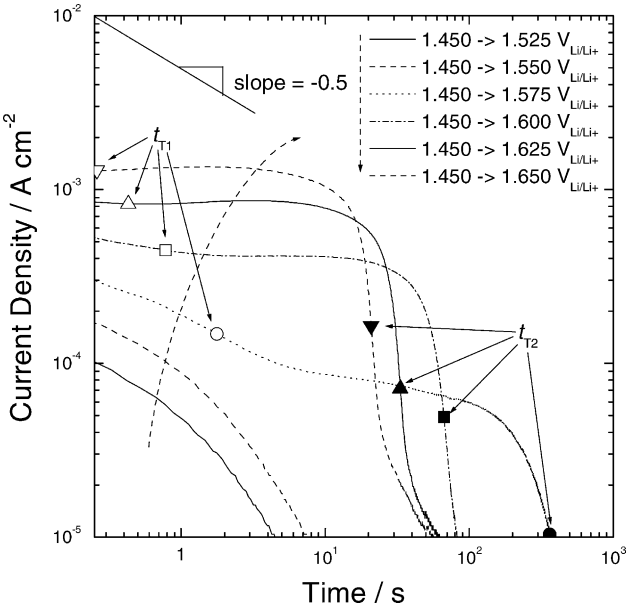

Fig. 3. Anodic current transients experimentally obtained from the $Li[Ti_{5/3}Li_{1/3}]O_4$ film electrode in a 1 M $LiClO_4$–PC solution by jumping the initial potential 1.450 V_{Li/Li^+} to various lithium extraction potentials as presented in figure. The first inflection points t_{T1} and the second inflection points t_{T2} are indicated by the open and closed symbols, respectively.

in the time interval between the first inflection point t_{T1} and the second inflection point t_{T2}, and finally did an exponential decay.

In our previous works [5–8], the non-Cottrell behaviour of the current transients measured on the transition metal oxides is responsible for the cell-impedance-controlled lithium transport through the oxides. In the cell-impedance-controlled model, the current is linearly proportional to the quotient of the potential difference between the electrode potential and the applied potential divided by the cell-impedance. The cell-impedance means the total internal cell resistance, major sources of which may be the bulk electrolyte, electrolyte/electrode interface, and bulk electrode. Under the circumstances, the current transient was theoretically calculated for the $Li[Ti_{5/3}Li_{1/3}]O_4$ film electrode by the Monte Carlo method under the cell-impedance-controlled constraint at the electrode surface well established in the previous work [22].

Fig. 4(a) gives on a logarithmic scale the current transients, theoretically calculated in consideration of the repulsive interactions between lithium ions under the cell-impedance-controlled constraint. The flux of lithium ions at the electrode surface and the Monte Carlo step (MCS) time were reduced by the total number of sites on the electrode surface side and the square of the total number of sites in the thickness direction perpendicular to the electrode surface, respectively. The current transients theoretically calculated by jumping 1.450 V_{Li/Li^+} to 1.600 and 1.625 V_{Li/Li^+} showed the wide current plateau followed by the abrupt decay in the time interval between t_{T1} and t_{T2}, which well coincided in shape with those current transients

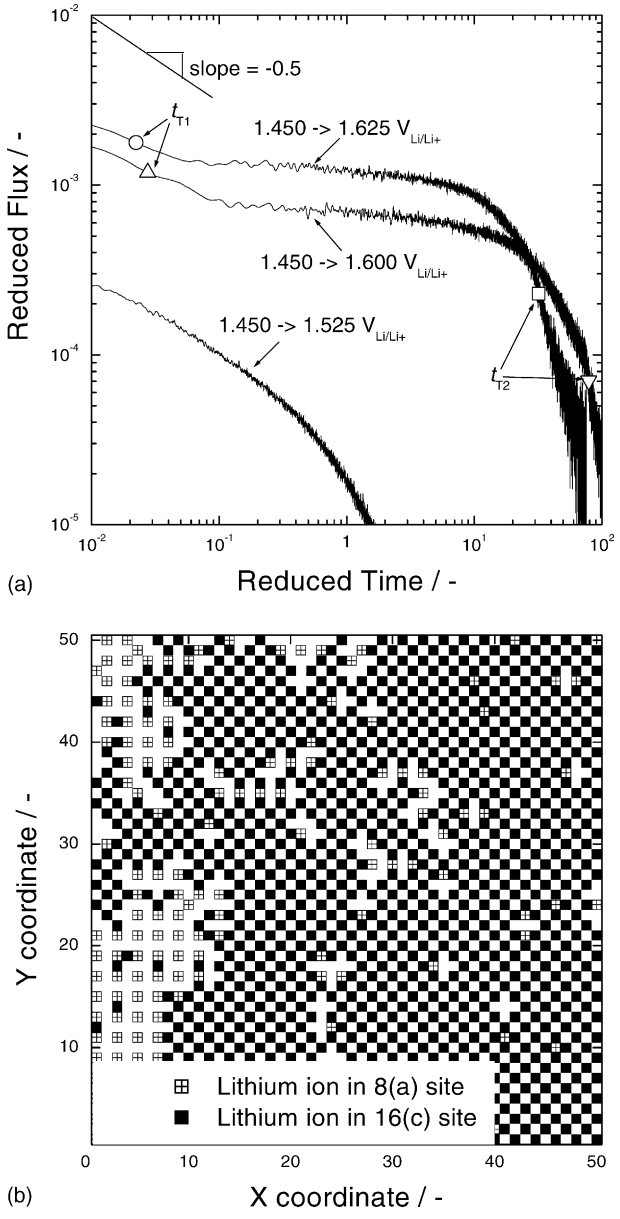

Fig. 4. (a) Anodic current transients theoretically calculated for the $Li[Ti_{5/3}Li_{1/3}]O_4$ film electrode by jumping the initial potential 1.450 V_{Li/Li^+} to the lithium extraction potentials 1.525, 1.600 and 1.625 V_{Li/Li^+} under the cell-impedance-controlled constraint. (b) Local cross-sectional snapshot of the configuration of lithium ions in the electrode simulated at $t_{T1} < t < t_{T2}$ by the Monte Carlo method.

experimentally measured (Fig. 3). From the results, it was suggested that lithium transport through the film electrode is governed by the cell-impedance-controlled constraint with the repulsive interactions between lithium ions.

In order to envisage the phase transformation of α to β and vice versa during the cell-impedance-controlled lithium transport, the local cross-sectional snapshot of the configuration of lithium ions was simulated by the Monte Carlo method [22]. Fig. 4(b) presents the local cross-sectional snapshot of the configuration of lithium ions obtained in the time interval between t_{T1} and t_{T2}. In the case of diffusion-

controlled lithium transport in the two-phase coexistence region it was previously suggested [23] that α phase which entirely covers the surface of β matrix, grows in the thickness direction toward the interface between the electrode and the current collector during the lithium deintercalation. However, in the case of cell-impedance-controlled lithium transport, it was found that α phase which is sporadically embedded in β matrix at the electrode surface, grows in both thickness and lateral directions during the lithium deintercalation as shown in Fig. 4(b).

In conclusion, from the thermodynamic approach to the lithium intercalation into the $Li[Ti_{5/3}Li_{1/3}]O_4$ film electrode with the help of the Monte Carlo method, it was proposed that the wide potential plateau in the electrode potential curve indicates the coexistence of the Li-poor phase α and the Li-rich phase β due to the repulsive interactions between lithium ions. From the kinetic approach, it was also suggested that transport of lithium ions which undergo the repulsive interactions with each other, occurs in the two-phase coexistence region under the cell-impedance-controlled constraint at the electrode surface.

Acknowledgements

This research was supported by a grant from the Center for Advanced Materials Processing (CAMP) of the 21st Century Frontier R&D Program funded by the Ministry of Science and Technology, Republic of Korea. Furthermore, this work was partly supported by the Brain Korea 21 project.

References

[1] W. Weppner, R.A. Huggins, J. Electrochem. Soc. 124 (1977) 1569.
[2] C.J. Wen, B.A. Boukamp, R.A. Huggins, W. Weppner, J. Electrochem. Soc. 126 (1979) 2258.
[3] A.J. Vaccaro, T. Palanisamy, R.L. Kerr, J.T. Maloy, J. Electrochem. Soc. 129 (1982) 682.
[4] S.-I. Pyun, S.-W. Kim, H.-C. Shin, J. Power Sources 81–82 (1999) 248.
[5] H.-C. Shin, S.-I. Pyun, Electrochim. Acta 45 (1999) 489.
[6] H.-C. Shin, S.-I. Pyun, S.-W. Kim, M.-H. Lee, Electrochim. Acta 46 (2001) 897.
[7] M.-H. Lee, S.-I. Pyun, H.-C. Shin, Solid State Ionics 140 (2001) 35.
[8] S.-I. Pyun, S.-W. Kim, J. Power Sources 97–98 (2001) 371.
[9] G.D. Smith, Numerical Solution of Partial Differential Equations: Finite Difference Methods, Oxford University Press, New York, 1987.
[10] T. Ohzuku, A. Ueda, N. Yamamoto, J. Electrochem. Soc. 142 (1995) 1431.
[11] S. Scharner, W. Weppner, P. Schmid-Beurmann, J. Electrochem. Soc. 146 (1999) 857.
[12] R. Darling, J. Newman, J. Electrochem. Soc. 146 (1999) 3765.
[13] S.-W. Kim, S.-I. Pyun, Electrochim. Acta 46 (2001) 987.
[14] W.R. McKinnon, R.R. Haering, in: R.E. White, J.O.M. Bockris, B.E. Conway (Eds.), Modern Aspects of Electrochemistry, vol. 15, Plenum Press, New York, 1983, pp. 235–304.
[15] T. Ohzuku, K. Tatsumi, N. Matoba, K. Sawai, J. Electrochem. Soc. 147 (2000) 3592.
[16] K. Binder, D.P. Landau, Phys. Rev. B 21 (1980) 1941.
[17] G. Ceder, Y.-M. Chiang, D.R. Sadoway, M.K. Aydinol, Y.-I. Jang, B. Huang, Nature 392 (1998) 694.
[18] Y. Gao, J.N. Reimers, J.R. Dahn, Phys. Rev. B 54 (1996) 3878.
[19] A. Van der Ven, C. Marianetti, D. Morgan, G. Ceder, Solid State Ionics 135 (2000) 21.
[20] Y.-M. Choi, S.-I. Pyun, S.-I. Moon, Solid State Ionics 89 (1996) 43.
[21] J.-S. Bae, S.-I. Pyun, J. Mater. Sci. Lett. 13 (1994) 573.
[22] S.-W. Kim, S.-I. Pyun, Electrochim. Acta 47 (2002) 2843.
[23] H.-C. Shin, S.-I. Pyun, Electrochim. Acta 44 (1999) 2235.